

# *Post-passivation of multication perovskite with rubidium butyrate*

*José Carlos Germino,<sup>1,§</sup> Rodrigo Szostak,<sup>1,2,§</sup> Silvia G. Motti,<sup>3</sup> Raphael F. Moral,<sup>1</sup> Paulo E. Marchezi,<sup>1</sup> Heitor S. Selegihini,<sup>1</sup> Luiz G. Bonato,<sup>1</sup> Francineide Lopes de Araújo,<sup>1</sup> Teresa D. Z. Atvars,<sup>1</sup> Laura M. Herz,<sup>3</sup> David Fenning,<sup>4</sup> Anders Hagfeldt<sup>2</sup> and Ana Flávia Nogueira<sup>1,\*</sup>*

<sup>§</sup> The authors contributed equally to this work

\*Corresponding author: [anafla@unicamp.br](mailto:anafla@unicamp.br)

<sup>1</sup> University of Campinas (UNICAMP), Laboratório de Nanotecnologia e Energia Solar, Chemistry Institute, Campinas, PO Box 6154, 13083-970, Brazil.

<sup>2</sup> Laboratory of Photomolecular Science, Institute of Chemical Sciences and Engineering, École Polytechnique Fédérale de Lausanne, 1015, Lausanne, Switzerland

<sup>3</sup> Department of Physics, University of Oxford, Clarendon Laboratory, Parks Road, Oxford OX1 3PU, United Kingdom.

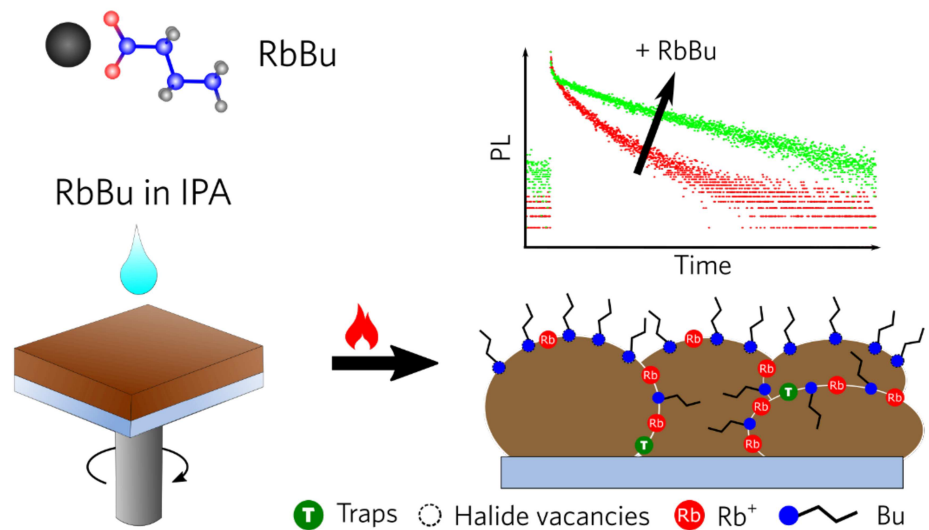
<sup>4</sup> Department of Nanoengineering, University of California, San Diego, La Jolla, CA 92093, USA.

## **Abstract**

Many multication perovskites for highly stable and efficient solar cells benefit from rubidium iodide introduced in the precursor solution. It is well known that  $\text{Rb}^+$  influences positively the optoelectronic and mobility properties and has a direct effect upon crystallization and halide homogenization. As  $\text{Rb}^+$  is often incorporated by adding  $\text{RbI}$  in the precursor solution, it can be difficult to distinguish the influence of  $\text{Rb}^+$  and  $\text{I}^-$  separately. Herein, we report a post-passivation of methylammonium-free (CsFA) perovskite films with rubidium butyrate (RbBu). The passivation with RbBu increases the hydrophobicity of the perovskite surface and passivates shallow and deep traps, leading to an increase of charge-carrier lifetimes and diffusion lengths. Consequently, a better photovoltaic performance is also observed. These superior properties are attributed to both surface (halide-vacancy) and grain-boundary passivation by the carboxylate group and  $\text{Rb}^+$ , respectively. We found that  $\text{Rb}^+$  itself acts as a direct and powerful passivating agent for multication perovskites, and this is proven by decoupling its contribution and halide's contribution to other important performance parameters (e.g. crystallization, halide vacancies filling, etc).

**Keywords:** Perovskite solar cells; surface-trap passivation; rubidium; THz pump-probe; perovskite defects; diffusion lengths.

## TOC Graphics –



## Main Text

Lead halide perovskites (LHPs) are an emerging class of materials that have drawn enormous attention from the scientific and engineering communities. Their tolerance to defects, long carrier lifetimes and diffusion lengths,<sup>1-3</sup> high absorption coefficients<sup>4</sup>, and composition-tunable bandgaps<sup>5</sup> are among the most remarkable of their properties. In addition, LHPs present easy processability, low production cost, and adaptability to flexible substrates, which make them promising materials for photonic devices such as solar cells, light-emitting diodes, lasers, detectors. The power conversion efficiency (PCE) of perovskite-based solar cells (PSCs) has increased from 3.9 %<sup>6</sup> to 25.2 %<sup>7</sup> on a lab-scale in a short period of time.

The most efficient and promising perovskites (ABX<sub>3</sub>) are composed of a mixture of organic cations such as methylammonium (MA<sup>+</sup>) and formamidinium (FA<sup>+</sup>) with small amounts of cesium (Cs<sup>+</sup>) on the A-site; Pb<sup>2+</sup> on the B-site; and iodide (I<sup>-</sup>) and bromide (Br<sup>-</sup>) anions on the X-site. PSCs based on these compositions have reached PCE above 20 %.<sup>8-10</sup> Also, the incorporation of small amounts ( $\approx$  5 %) of alkali metal ions (Li<sup>+</sup>, Na<sup>+</sup>, K<sup>+</sup> and Rb<sup>+</sup>) have improved even further the photovoltaic performance and stability.<sup>11,12</sup> Doping with the alkali metal Rb<sup>+</sup> was first introduced by Saliba *et al.*<sup>13</sup> for CsFAMAPb(I/Br) perovskite, with solar cells reaching a PCE of 21.6%. The better performance in comparison with the reference device was reached mainly by an increase in the open circuit potential voltage, indicating a reduction in charge-carrier recombination as observed for other compositions with Rb<sup>+</sup> as well.<sup>14-18</sup> Hu *et al.*<sup>19</sup> showed that the superior performance of Rb<sup>+</sup> when incorporated in the perovskite could be assigned to the reduction of traps and enhancement of charge-carrier mobility. Using solid-state NMR, Kubick *et al.*<sup>20</sup> found no proof that Rb<sup>+</sup> was incorporated into the perovskite structure, but it occurred but it occurred as a RbPb(I<sub>x</sub>Br<sub>1-x</sub>)<sub>3</sub> second phase, confirmed later by other studies.<sup>21,22</sup> On the other hand, Cao *et al.*<sup>23</sup>

experimentally demonstrated a lattice expansion when  $\text{Rb}^+$  is incorporated to CsFAMA indicating an interstitial occupancy. Density function theory (DFT) calculations supported interstitial positioning of  $\text{Rb}^+$  and other smaller cations ( $\text{K}^+$ ,  $\text{Na}^+$  and  $\text{Li}^+$ ), but only  $\text{Rb}^+$  is predicted to occupy, in minor extension, the A-site. Docampo *et al.*<sup>21</sup> observed the same lattice expansion for  $\text{Rb}^+$  incorporation; however, they attributed this effect to a reduction of  $\text{Br}^-$  in the perovskite by the formation of a Br-rich  $\text{RbPb}(\text{I}_x\text{Br}_{1-x})_3$  second phase, inducing the formation of I-rich bulk perovskite with larger lattice parameters. Opposing the two latter works, Tang *et al.*<sup>24</sup> reported no lattice changes when  $\text{Rb}^+$  was incorporated to FAMA; however, they observed lattice expansion for  $\text{Li}^+$ ,  $\text{Na}^+$ , and  $\text{K}^+$  in agreement with the work of Cao *et al.*<sup>23</sup> Interestingly, Qiao *et al.*<sup>25</sup> theoretically studied the introduction of alkali metal together with interstitial iodide, which is well known to create deep traps; they concluded that these traps can be eliminated by alkali addition. It is clear that, besides the positive effects of the  $\text{Rb}^+$ , the real mechanism that leads to the superior optoelectronic properties has not been fully unravelled yet.

Furthermore, so far, all studies on Rb-modified perovskites were carried out by the introduction of  $\text{RbI}$  in the perovskite precursor solution, complicating a distinction between the contribution from the alkali cation and the halide. *In situ* grazing incidence wide angle X-ray scattering (GIWAXS) analysis during spin coating preparation confirmed that the addition of  $\text{RbI}$  in the perovskite solution reduces the formation of non-perovskite, hexagonal phases (2H, 4H, and 6H), improving the performance of the devices.<sup>26,27</sup> In other words,  $\text{RbI}$  plays an important role in dictating the intermediates and, consequently, the crystallization paths. This happens because the colloidal size of the polyhalides, which are initially formed, depends on the proportion of cation and halide (excess of MAI,  $\text{M}\text{A}\text{Cl}$ ) or halide acids (addition of  $\text{HBr}$ ,  $\text{HI}$ ) used in the precursor solution.<sup>28–30</sup> Moreover, the higher amount of the halide introduced together with  $\text{Rb}^+$  can fill the halide vacancies, further improving the

optoelectronic properties.<sup>31</sup> Yang *et al.*<sup>32</sup> showed that the introduction of additional iodide ions into the organic cation solution decreases the concentration of deep-level defects. Recently, Correa-Baena *et al.*<sup>33</sup> found that the addition of RbI has led to halide homogenization, which coincides with long-lived charge-carrier decays, revealing an effect not directly related to Rb<sup>+</sup> alone.

Analyzing the aforementioned publications raises the question if the improved optoelectronic properties observed by the addition of RbI comes from the direct passivation by Rb<sup>+</sup> and I<sup>-</sup> (or both), and/or from an effect on the crystallization and film formation. To definitively assign the benefits of Rb<sup>+</sup> incorporation, we prepared an isopropanol-soluble rubidium butyrate (RbBu) and used post-passivation of the Cs<sub>0.10</sub>FA<sub>0.90</sub>Pb(I<sub>0.83</sub>Br<sub>0.17</sub>)<sub>3</sub> perovskite. This approach allowed us to visualize the effect of the Rb<sup>+</sup> and the anion without their influence on the perovskite crystallization and final morphology. The XRD analysis revealed no change in the bulk perovskite by passivation and the formation of  $\delta$ -RbPb(Br<sub>x</sub>I<sub>1-x</sub>)<sub>3</sub> side phase only when a higher concentration of RbBu was used. The Bu<sup>-</sup> passivation at the surface was evidenced by the increase in contact angle and higher moisture resistance due to the hydrophobic character of the butyrate carbon chain. RbBu passivation also reduced the trap density, increasing the charge-carriers lifetime and diffusion length, and leading to better device performance with reduced hysteresis. The charge-carrier diffusion lengths increased from 3.69 to 5.00  $\mu$ m, when comparing pristine and 5 mM passivated samples, respectively. This improvement was attributed to Bu<sup>-</sup> passivation of the undercoordinated Pb<sup>2+</sup> (halide vacancies) at the film surface and Rb<sup>+</sup> passivation of deep-traps located at grain boundaries. Our studies reveal the positive role of the Rb<sup>+</sup> in grain boundary passivation unrelated to other ambiguous effects such as crystallization.

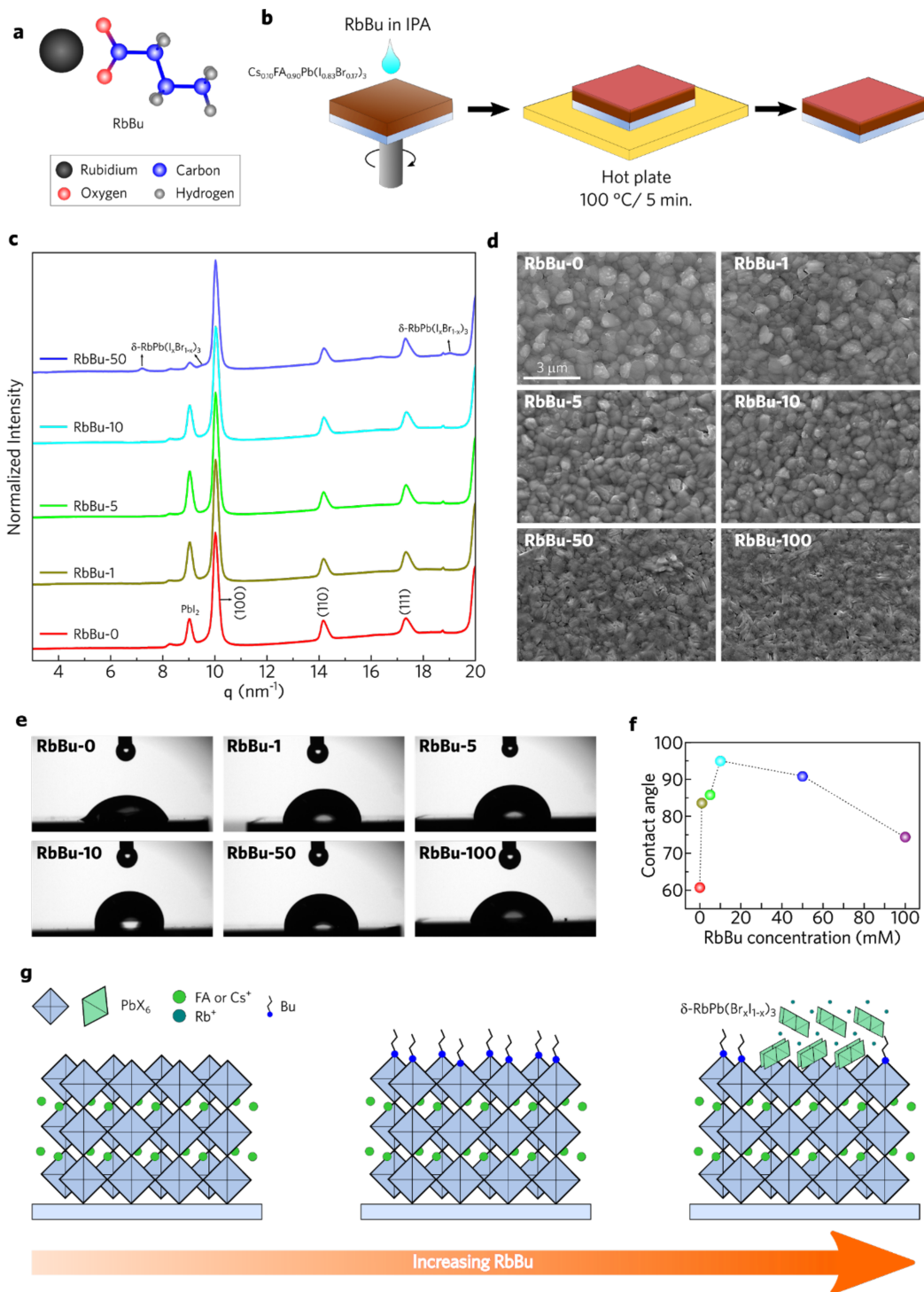


**Figure 1.** (a) Molecular structure of the rubidium butyrate (RbBu); (b) Schematic representation of the perovskite passivation by RbBu; (c) XRD patterns of the pristine and passivated perovskite films; (d) SEM images; (e) contact angle images; and (f) contact angle as a function of the RbBu concentration. (g) Scheme showing the effect of the RbBu passivation as the concentration of RbBu increases.

To perform the perovskite passivation with Rb, rubidium butyrate salt (RbBu, Figure 1a) was synthesized as described in the Supporting Information. Unlike RbI, which is insoluble, RbBu presents high solubility in isopropanol (IPA). This allows a post-passivation of the bulk perovskite, similar to the method used for other passivating studies.<sup>34-36</sup> RbBu was dissolved in different concentrations (1, 5, 10, 50 and 100 mM) in IPA and dripped on the pristine  $\text{Cs}_{0.10}\text{FA}_{0.90}\text{Pb}(\text{Br}_{0.17}\text{I}_{0.83})_3$  perovskite film during spin coating. Afterwards, the films were thermally annealed to complete the passivation (Figure 1b).

Figure 1c shows the X-ray diffraction (XRD) patterns of the pristine (RbBu-0) and RbBu-modified (RbBu-X, X = the concentration of RbBu in IPA) perovskite films obtained by grazing-incidence wide-angle X-ray scattering. The RbBu-0 pattern reveals peaks from pseudo-cubic perovskite at  $q = 10.03$ ,  $14.17$  and  $17.35 \text{ nm}^{-1}$ , consistent with previous reports.<sup>37</sup> The peak from  $\text{PbI}_2$  at  $q = 9.04 \text{ nm}^{-1}$  is also observed due to an excess of  $\text{PbI}_2$  intentionally introduced during the perovskite preparation. It is well known that excess of  $\text{PbI}_2$  improves the perovskite film quality.<sup>38-40</sup> With RbBu passivation, the peaks from the perovskite remain unchanged with no peak shift (see Figure S1). This indicates that  $\text{Rb}^+$  is not incorporated into the interstitial sites of the bulk perovskite, unlike the report by Cao *et al.*<sup>23</sup>, where addition of 2% of RbI into the perovskite solution led to a peak shift. Therefore, we expect to find  $\text{Rb}^+$  mainly on the surface, between grain boundaries, or in very low concentrations inside of the crystal lattice, which is not detectable by XRD analysis. The peak from  $\text{PbI}_2$  increases, reaching its maximum for RbBu-5, and then decreases. The increase of the  $\text{PbI}_2$  peak intensity is attributed to partial dissolution of the FA molecules on the surface of the perovskite films by IPA during the post-passivation treatment, as suggested by Yoo *et al.* for 2D/3D perovskite surface treatment.<sup>41</sup> For the sample RbBu-50, small peaks at  $q = 7.22$ ,  $\sim 9.50$  and  $\sim 19.00 \text{ nm}^{-1}$ , attributed to non-perovskite phase  $\delta\text{-RbPb}(\text{Br}_x\text{I}_{1-x})_3$ ,

emerged, indicating that, above a certain concentration,  $\text{Rb}^+$  reacts with excess of  $\text{PbI}_2$ , forming  $\delta\text{-RbPb}(\text{Br}_x\text{I}_{1-x})_3$  detectable by XRD. The surface morphology of the samples was evaluated by scanning electron microscopy (SEM), and the images are shown in Figure 1d. The morphology of RbBu-0 perovskite reveals grains with size between 0.4 and 1.2  $\mu\text{m}$ . The application of up to 10 mM of RbBu did not significantly change the morphology of the films; however, the RbBu-50 and RbBu-100 samples present rod-like crystals. We assign these structures to  $\delta\text{-RbPb}(\text{Br}_x\text{I}_{1-x})_3$ , in accordance with the XRD and supported by solid-state  $^{87}\text{Rb}$ -MAS-NMR analyses for the RbBu-100 sample (Figure S2 and Supporting Text 1).

Besides  $\text{Rb}^+$ , it is expected that the butyrate anion plays an important role in both passivation and hydrophobicity of the films. To evaluate the butyrate effect on the hydrophobicity, we measured the contact angle for all samples. Figure 1e and 1f show the images of water droplets on the perovskite surface and the contact angle variation with different concentrations of RbBu, respectively. The variation to higher contact angles clearly reveals an increase in hydrophobicity after RbBu passivation, with maximum angle obtained for RbBu-10 ( $95^\circ$ ). Additionally, the Supporting Video 1 shows a persistent water-repellent effect in the RbBu-10 sample, in contrast to the RbBu-0. While the post-treated sample persists with the water drop at an angle of  $\sim 90^\circ$  during the entire recording time the water drops spread over the film instantly in the non-modified sample. For higher concentrations of RbBu (RbBu-50 and RbBu-100), the contact angle decreases; this change may be related to the formation of  $\delta\text{-RbPb}(\text{Br}_x\text{I}_{1-x})_3$ , which increases the hydrophilicity of the films. The water repellent property was also confirmed by sample exposition to ambient conditions for two weeks as shown in Figure S3. Even the lower concentration of RbBu led to an improvement of perovskite stability against ambient moisture, and the most resistant film was RbBu-10, which presented the higher contact angle. Figure 1g summarizes the RbBu passivation in relation to its concentration during preparation. For intermediate concentration

of RbBu, the Bu anion is bonded on the surface, leading to a hydrophobic character; however, for high concentrations, the formation of  $\delta$ -RbPb( $\text{Br}_x\text{I}_{1-x}$ )<sub>3</sub> takes place, leading to a hydrophilic character.

The optical properties and the charge-carrier dynamics of the pristine and modified films with RbBu were evaluated by steady-state absorption and steady-state photoluminescence (PL), as well as time-resolved photoluminescence (TRPL) transients acquired by time-correlated single-photon counting (TCSPC) measurements. The addition of RbBu on the surface of the perovskite films leads to a discrete blue-shift in the band-edge of their absorption spectra, yielding an isosbestic point at  $\lambda_{\text{abs}} = 740$  nm (Figure S4). Similarly, the PL spectra (Figure 2a) of the modified perovskite thin-films exhibited a small blue-shift (about 10 nm) at its maximum photoluminescence wavelength ( $\lambda_{\text{PL}}$ ) with the increment of the RbBu content ( $\lambda_{\text{PL}}(\text{RbBu-0}) = 766$  nm to  $\lambda_{\text{PL}}(\text{RbBu-100}) = 756$  nm). This blue-shift and the isosbestic point in the UV-Vis spectra are probably related to the formation of  $\delta$ -RbPb( $\text{Br}_x\text{I}_{1-x}$ )<sub>3</sub>.

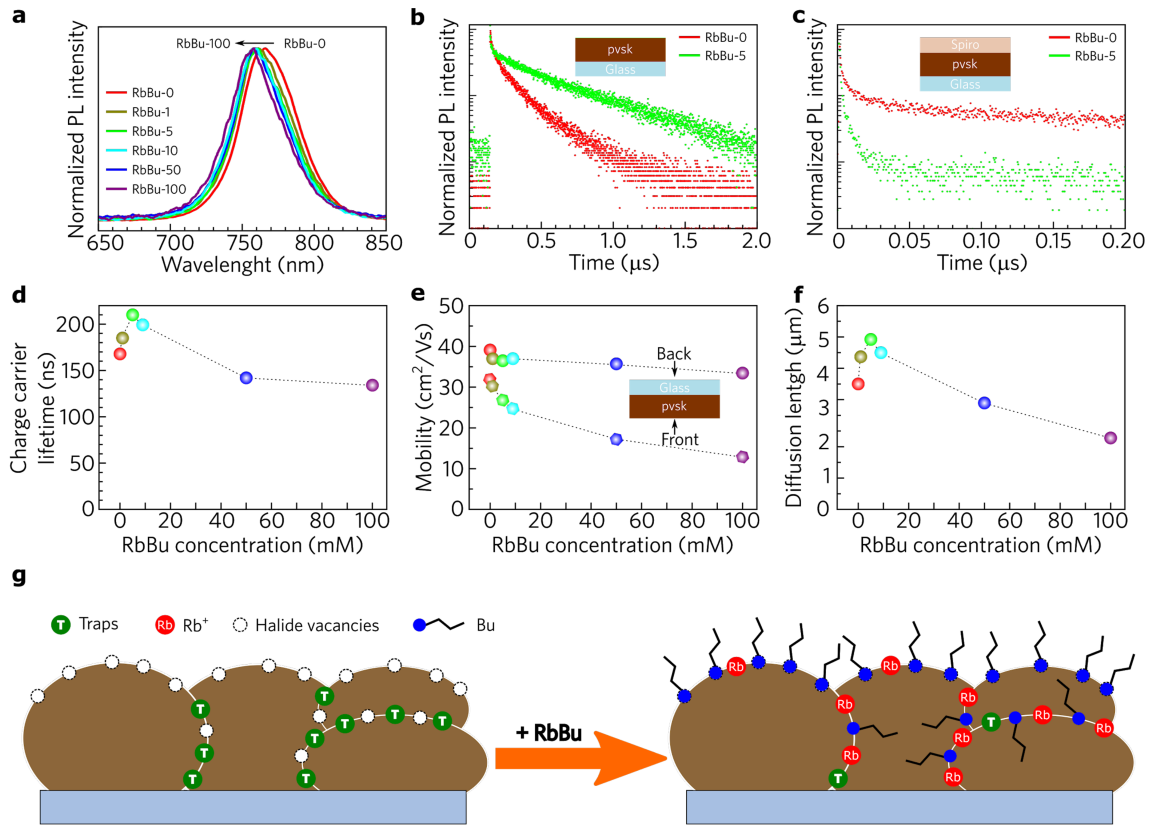


**Figure 2.** (a) PL ( $\lambda_{\text{exc}} = 442$  nm, CW) spectra; (b and c) charge-carrier dynamics revealed by TRPL on films without and with Spiro-OMeTAD, respectively ( $\lambda_{\text{exc}} = 440$  nm,  $F = 9.7$  nJ  $\text{cm}^{-2}$ ); (d) charge-carrier lifetimes as a function of RbBu concentration; (e) electron-hole sum mobilities from optical-pump terahertz-probe (OPTP) measurements; data was acquired either for front or back excitation of the films. (f) Charge-carrier diffusion lengths considering front face excitation as a function of RbBu concentration. (g) Schematic representations of the passivation by RbBu.

Commonly, the total charge-carrier recombination in LHPs is described by a high-order dynamics equation, where the charge-carrier density ( $n$ ) is a time ( $t$ ) function controlled by the monomolecular trap-assisted, bimolecular band-to-band, and Auger recombination phenomena.<sup>42</sup> Nevertheless, it is well known that the contribution of the high-order charge-carrier dynamics cannot be accessed at low-fluence regimes, due to the low charge-carrier density generated by the excitation,<sup>43</sup> as in our time-correlated single photon counting

(TCSPC) experiments ( $F = 9.7 \text{ nJ cm}^{-2}$ ,  $n_0 \approx 10^{14} \text{ cm}^{-3}$ ). Thus, a single-exponential emission decay should be observed from the TCSPC. However, a monoexponential function does not adequately represent the TRPL decays (Figures 2b) due to the disorder of the perovskite films (*i.e.*, grain size distribution, multi-cation composition, Br- and I-rich phases segregation, high-density of trap-states, etc.) and processing conditions, in addition to effects of diffusion dynamics. Therefore, a stretched exponential decay function was used to extract the charge-carrier lifetimes, and the details of the fit are in the Supporting Text 2 and Table S1.

As a general trend, the addition of the RbBu additive increases the charge carrier lifetime, and the RbBu-5 composition exhibited the maximum lifetime ( $\tau_s = 210 \text{ ns}$ ); an enhancement of about 25 % in relation to the lifetime of non-modified LHP ( $\tau_s = 168 \text{ ns}$ ). Above this concentration (RbBu-10 and higher), the charge carrier lifetime decreases until  $\tau_s = 134 \text{ ns}$  (RbBu-100 - see Table S1). An enhancement of the emission lifetime was already observed for mixed-halide perovskites as a function of the RbI content in alloyed LHP, and our results corroborate with their findings.<sup>33</sup> In addition, Figure 2c presents the TRPL decays of the RbBu-0 and RbBu-5 samples with a layer of the HTM on the top of the film. A more efficient hole extraction can be observed in the RbBu modified films when the Spiro-OMeTAD layer is present, in comparison to the non-modified film. The faster PL decay in the RbBu-5 sample is directly related to the decrease of the interface mismatching between the perovskite surface and the HTM organic layer. The presence of the Bu- anions on the surface of the grains (Figure 2g) improves the compatibility of the Spiro-OMeTAD layer with the perovskite material.

To further understand the effect of Rb<sup>+</sup> we performed additional PL measurements. We prepared perovskite films adding RbBu and RbI (5%) inside the perovskite precursor solution. Figure 3 compares the TRPL of pristine perovskite (RbBu-0), perovskite with RbBu post passivation (RbBu-5), RbBu inside the solution (CsFA + 5% RbBu), and RbI inside the

solution (CsFA + 5% RbI). Because of the insolubility of RbI in IPA, it was not possible to carry out a post passivation similar to RbBu. As expected, the addition of RbI inside solution increased the lifetime similar to RbBu-5 passivation ( $\tau_{s(\text{CsFA} + 5\% \text{RbI})} = 211 \text{ ns}$ ). Interestingly, the addition of RbBu inside the perovskite solution led to a slight increase of lifetime in comparison to pristine sample ( $\tau_{s(\text{CsFA} + 5\% \text{RbBu})} = 172 \text{ ns}$ ), but it is not comparable to the RbBu-5 and CsFA + 5% RbI, indicating that the halide anion is also contributing to defect passivation.

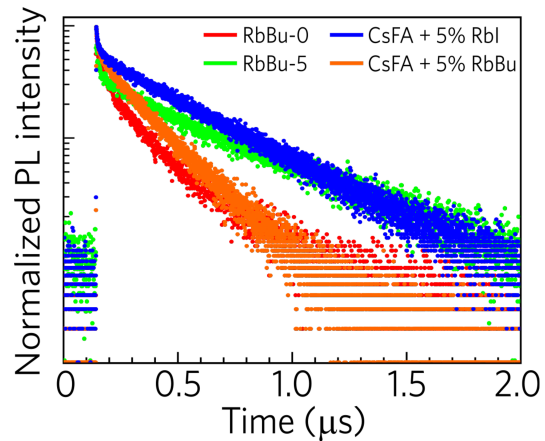


**Figure 3.** Comparison between TRPL decays of RbBu-0, RbBu-5, CsFA + 5 % RbI in solution, and CsFA + 5 % RbBu in solution ( $\lambda_{\text{exc}} = 440 \text{ nm}$ ;  $\lambda_{\text{PL}} = 760 \text{ nm}$ ;  $F = 9.7 \text{ nJ cm}^{-2}$ ).

To investigate the effect of the RbBu on the charge transport, we carried out the optical-pump terahertz-probe (OPTP) and extract the THz charge-carrier mobility ( $\mu$ ) values, following the method described by Wehrenfennig *et al.*<sup>44</sup> The OPTP measurements were performed with photoexcitation from either the perovskite film side (front) or on the substrate side (back), and the values of the electron-hole sum mobilities obtained are depicted in Figure 2e. The 400 nm photoexcitation employed results in an initial concentration of charge-carriers close to the illuminated side. Thus, the measurements performed for excitation from either side of the film can selectively probe the carrier mobilities in the vicinity of each passivated or non-passivated surface.<sup>45</sup> As a general trend, the electron-hole sum mobility

drops with the passivation, from  $\mu_{(0 \text{ mM})} = 31.9 \pm 1.2 \text{ cm}^2 \text{ V}^{-1} \text{ s}^{-1}$  to  $\mu_{(100 \text{ mM})} = 12.9 \pm 2.1 \text{ cm}^2 \text{ V}^{-1} \text{ s}^{-1}$ , exhibiting a dependence of the RbBu concentration, mainly for the front-face photoexcitation measurements. A decrease of the  $\mu$  values can also be observed for the measurements performed on the back-face excitation conditions; however, to a much lower extent ( $\mu_{(0 \text{ mM})} = 39.1 \pm 0.9 \text{ cm}^2 \text{ V}^{-1} \text{ s}^{-1} \rightarrow \mu_{(100 \text{ mM})} = 33.4 \pm 0.3 \text{ cm}^2 \text{ V}^{-1} \text{ s}^{-1}$ ). It reveals that RbBu can penetrate in the film but the most remains near the surface of the perovskite film.

Taking into account the balance between the decrease of the trap-assisted recombination rates ( $k_I$ ), the decrease of the charge-carrier mobility on the perovskite films, and how these effects impact on the PSCs performance, a useful quantity to state the overall improvement of the devices is the diffusion length ( $L_D$ ) of the charge-carriers.  $L_D$  values were estimated from equation 1:

$$L_D = \left( \frac{\mu k_B T}{e k_1} \right)^{\frac{1}{2}} \quad (1)$$

where  $k_B$  is the Boltzmann constant,  $T$  is the temperature, and  $e$  is the elementary charge. At low fluence regimes and charge-carrier lifetimes varying from  $100 \text{ ns} < \tau_S < 1000 \text{ ns}$  ( $10^6 \text{ s}^{-1} < k_I < 10^7 \text{ s}^{-1}$ ),  $L_D$  has a minor dependence on the charge-carrier density ( $n$ ).<sup>44</sup> In this way, the total charge-carrier recombination rate can be approximated to be  $k_I$ , and the obtained values of  $L_D$  are summarized in Figure 2f and Table S1. As a general trend, the  $L_D$  values of the modified thin-films with RbBu increase with the surface passivation up to the concentration of 5 mM, from  $L_{D(0 \text{ mM})} = 3.69 \text{ } \mu\text{m}$  to  $L_{D(5 \text{ mM})} = 5.00 \text{ } \mu\text{m}$ . Above that concentration, the charge-carrier diffusion length decreases to values ( $L_{D(100 \text{ mM})} = 2.10 \text{ } \mu\text{m}$ ), lower than those for the non-modified perovskite. The trend observed for the charge-carrier dynamics indicates that the ideal concentration of RbBu surface additive is 5 mM.

It is clear from our data that the charge-carrier dynamics change after RbBu passivation. As pointed out earlier, the choice of a post-passivation by a non-halide  $\text{Rb}^+$  precursor was intended to separate the influence of the alkali metal and the halide on passivation as well as on the perovskite crystallization and morphology.  $\text{Bu}^-$  anion is expected to behave differently when compared with the halides (I and Br).  $\text{Bu}^-$  presents a carboxyl group ( $\text{COO}^-$ ) with negative charge distributed on the two oxygen atoms (See Figure S9) bonded to an inert carbon chain. Hence,  $\text{Bu}^-$  anions ( $V_{\text{Bu}} = 137 \text{ \AA}^3$ ; see DFT calculations in the SI) are larger than iodide and bromide ( $V_{\text{I}^-} = 44 \text{ \AA}^3$  and  $V_{\text{Br}^-} = 31.5 \text{ \AA}^3$ ). Because of their larger size, it is not expected that  $\text{Bu}^-$  ions penetrate the bulk perovskite and occupy halide vacancies or interstitials. Recently, Park *et al.*<sup>46</sup> reported that carboxylic acids do not penetrate metal halide perovskite, remaining mainly on the surface. In our study, the decrease in the charge-carrier mobility upon RbBu incorporation can only be attributed to the insulating character of the  $\text{Bu}^-$ .

Despite the fact that  $\text{Bu}^-$  anions remain mainly on the surface, passivating the undercoordinated  $\text{Pb}^{2+}$  cations, some of them may penetrate between the grain boundaries (Figure 2g). In our case,  $\text{Bu}^-$  anions incorporated in between the grains seem to hinder the charge-carries mobility, as observed in the OPTP measurements. Regardless of causing a minimal impact on mobility, the synergistic effect of Pb-Bu passivation and the increase in the hydrophobicity, which improves stability against moisture (Figure S3), are important benefits revealed by our approach.

The intermediate size of  $\text{Rb}^+$  allows it to occupy interstitials or the A-site.<sup>23</sup> Our XRD analysis shows no shifts in the peak positions or lattice expansion, indicating that  $\text{Rb}^+$  seems not to be incorporated into the bulk. However, the higher charge-carrier lifetimes and diffusion length after passivation indicate the possibility that deep traps are being passivated. Recent studies have reported that the main portion of the traps in mixed halide perovskites

are located between grains with inhomogeneous Br and I distribution.<sup>47-48</sup> Theoretical studies have demonstrated that the main defects formed in perovskites are interstitial halogen ( $I_i$  and  $Br_i$ ) defects and vacancies of lead ( $V_{Pb}$ ) and halides ( $V_I$  or  $V_{Br}$ ).<sup>49,50</sup> Among them,  $I_i$  (or  $Br_i$ ) is more detrimental and can significantly trap holes<sup>50-52</sup>. Deactivation of interstitial iodide deep traps was proposed when PCBM and oxygen interact with these defects.<sup>53-55</sup> We propose that a possible mechanism for  $Rb^+$  passivation is its binding to  $I_i$  (or  $Br_i$ ) at grain boundaries, which leads to a decrease in the hole-trap density by the formation of shallower states and, consequently, a lower hole trapping rate. This hypothesis is supported by a theoretical study which showed that alkali metals eliminate the deep traps in contact with interstitial halide defects.<sup>25</sup> To get more insight into  $RbBu$  passivation we carried out X-Ray photoelectron spectroscopy (XPS) and the results are discussed in more detail in supplementary text 3. In general, the  $Rb^+$  peaks emerged in sample  $RbBu$ -10 with one component, and another emerged for samples  $RbBu$ -50 and  $RbBu$ -100. The first component observed may be attributed to  $Rb^+$  passivating the interstitial halides defects and the second to  $\delta$ - $RbPb(Br_xI_{1-x})$ , also observed in XRD analysis.

Figure 2g (left side) schematically shows the location of the traps between the grain boundaries and also the halide vacancies at the surface that lead to undercoordinated  $Pb^{2+}$ . After the treatment with  $RbBu$ , these traps are passivated (Figure 2g, right side), and the  $Bu^-$  species tend to remain on the surface, whereas  $Rb^+$  is expected to penetrate further in the structure.

In summary, perovskite post-passivation with  $RbBu$  results in charges that diffuse longer because of  $Rb^+$  defect passivation but with lower mobility. The negative effect on the mobility is caused by the insulating nature of the butyrate anions. In other words, the effect on the charge diffusion length  $L_D$  caused by  $Rb^+$  addition surpasses the negative contribution in the mobility from the butyrate anion. In addition, it is clear that  $Rb^+$  alone does not improve

the optoelectronic properties of the perovskite, and the anion also plays an important role when the salts are added inside the solution. It is important to point out that the exact passivation mechanism that leads to higher charge diffusion length in this work is not clear, and further studies are necessary.

To evaluate the effectiveness of the RbBu passivation in the PSC performance and stability, we fabricated and characterized PSCs with planar architecture as shown in Figure 4a (glass|FTO|SnO<sub>2</sub>|perovskite|Spiro-OMeTAD|Au). For an accurate characterization, all devices were measured in backward and forward scanning and at maximum power point (MPP) for 1 minute. The results are summarized in Figure 4b-i and Table S2. The best control PSC (RbBu-0) reached 16.7% ( $15.5 \pm 0.7\%$ ) and 18.1% ( $16.9 \pm 0.8\%$ ) for forward and backward scans, respectively. While the short-circuit current densities of the modified samples are comparable with the control PSC (Figure 4g), the  $V_{oc}$  and FF increased with passivation, leading to better PCE and reduced hysteresis. The maximum PCE was obtained for RbBu-5, yielding 17.9 ( $17.7 \pm 0.2\%$ ) and 18.0 % ( $17.6 \pm 0.3\%$ ), for forward and backward scans, respectively. The best RbBu-5 PSC is shown in Figure 4c. Also, superior reproducibility of the devices was observed for devices where the perovskite film underwent passivation. Despite the modest improvement in PCE from JV scans, the PCE measured at MPP after 1 minute, shown in Figure 4h, reveals a superior performance of the devices with passivation. The RbBu-0 reached the average PCE at MPP of  $13.9 \pm 1.8\%$ , while RbBu-5 reached a lower limit of  $17.2 \pm 0.2\%$ . The increase in  $V_{oc}$  corroborates the TRPL analysis where the charge-carrier lifetime increased with RbBu passivation. It is expected that a reduction in mobility increases hysteresis.<sup>22,56</sup> However, we observed a decrease in the hysteresis, even for the sample with the smallest carrier mobility. We hypothesize that the carrier mobility is compensated by the reduction of surface trap states and because of the increase in hole extraction by Spiro-OMeTAD, as shown in TRPL measurements (Figure 2b

and 2c). It seems that the passivation has improved the wettability of the perovskite interface towards the HTM layer.

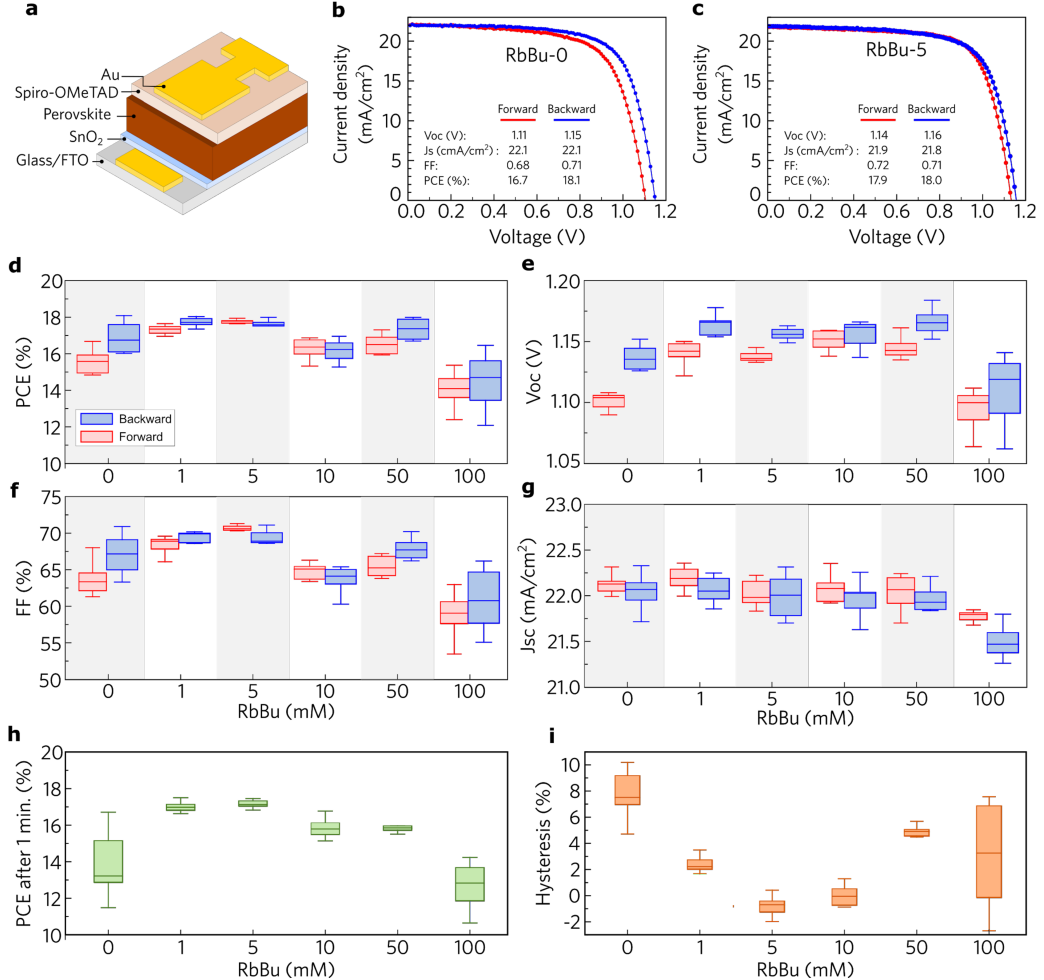


**Figure 4:** (a) The device architecture of n-i-p planar PSCs; J-V characteristics of (b) RbBu-0 and (c) RbBu-5 champion devices in forward and backward scans; (d) PCE; (e)  $V_{oc}$ ; (f) FF; (g)  $J_{sc}$  statistics for PSCs; (h) PCE at MPP after 1 minutes of stabilization; and (i) hysteresis index.

The device stability was verified by the performance at maximum power point (MPP) under continuous illumination in an inert atmosphere ( $N_2$ ). Figure S10a shows the results for CsFA perovskite during 120 h. The passivated perovskite device performed better initially however, after 120h, the PCE was similar for both devices. We also prepared devices with

CsFAMA perovskite (Figure S10b) to verify the effect of the perovskite composition, and the results revealed a similar trend: the passivated device yielded higher PCE in the first hours of testing but reduced to similar performance after 60 h. Despite the clear improvement in perovskite film stability (Figure S3) and performance of the freshly RbBu-passivated devices, the long-term stability had no clear improvement. Carboxyl groups passivation in perovskites are scarce, only reported for more complex molecules and, normally, in the protonated form.<sup>46,57-60</sup> Many studies do not present stability tests and, when presented, are not comparable and not carried out with continuous illumination and/or at MPP. Mostly, the perovskite passivation (introduced into solution or in a post-passivation treatment) is done using halide compounds, which reduces the halide vacancies in parallel with cation passivation or 2D layer formation. These approaches reduce halide diffusion in the bulk and at the interfaces of the perovskites, preventing device degradation under operation.<sup>61,62</sup> As discussed previously, it is not expected that the butyrate anions fill the halide vacancies in the bulk, but rather on the surface; consequently, similar degradation may occur for the pristine and passivated perovskites. Another possibility is that the the butyrate anions can be removed from the surface because of weak  $\text{COO}^-$ - $\text{Pb}^{2+}$  bonds. The chemical bond between  $\text{Bu}^-$  and perovskite can be rationalized using the Pearson acid-base concept. The carboxyl group of  $\text{Bu}^-$  is a hard base and  $\text{Pb}^{2+}$  is a borderline acid; therefore, a strong interaction is not expected. This behavior can indicate that  $\text{Bu}^-$  is weakly bonded to perovskite surface and, consequently, with a weak capacity to passivate and protect the surface under continuous illumination conditions with applied bias.

In conclusion, a new post-passivation method with isopropanol-soluble rubidium butyrate was applied to mixed-halide, mixed-cation perovskite thin films. This method allowed us to passivate the perovskite with  $\text{Rb}^+$  without the influence of both cation and anion on crystallization and morphology that is encountered when  $\text{RbI}$  is added to the precursor

solution, as had been widely reported previously. The passivation with RbBu led to an increase in the hydrophobicity of the perovskite film according to contact angle measurements and improved stability against moisture, effects attributed to the insulating nature of Bu<sup>-</sup> on the film surface. The presence of the Bu<sup>-</sup> also induces a decrease in the charge-carrier mobility upon passivation. However, the charge-carrier lifetime and diffusion length increased with passivation, indicating a reduction of traps states in perovskite. Since the Bu<sup>-</sup> cannot penetrate deeply in the bulk perovskite, the higher diffusion length is mainly attributed to Rb<sup>+</sup> and confirms the Rb<sup>+</sup> passivation, eliminating possible indirect effects on perovskite formation when it is added to the solution. These changes impact the photovoltaic performance of the devices: we observed a considerable PCE enhancement for the modified device, according to MPP experiments, mainly owing to the decrease of the device's hysteresis and the trap-assisted recombination rate. However, no clear evidence of the PSC stability improvement could be observed in our experiments, probably because of the weak interaction between Pb<sup>2+</sup> and Bu<sup>-</sup>.

Our work indicates that alkali metal post-passivation by isopropanol-soluble salts is a new strategy to reach similar and positive outcomes compared to the standard methods of LHPs fabrication, with an additional gain in separating the effect of both cation and anion on the optoelectronic properties as well their influence on perovskite formation/crystallization. This method can also be easily extended to other alkali cations with different counter-ions to provide a clear understanding of the role of these small cations on multication perovskite properties.

## Associated Content

### Supporting Information

Supporting information contains experimental details, materials, synthesis of RbBu, preparations of perovskite and surface modification, structural and optical characterization methods, PSCs assemble and characterization method, theoretical calculations, and additional characterization data, and supplementary texts 1, 2 and 3.

### Supporting Video 1.

## Acknowledgments

All authors thank the LNLS for providing beamtime at the XRD2. R. S. thanks São Paulo Research Foundation (FAPESP, Grant 2017/12582-5 and 2018/25801-0). R.F.M thanks to São Paulo Research Foundation (FAPESP, Grant 2019/25765-6). J. C. G and A. F. N. gratefully acknowledge the support from the FAPESP (Grant 2017/11986-5) and Shell and the strategic importance of the support given by ANP (Brazil's National Oil, Natural Gas and Biofuels Agency) through the R&D levy regulation. A. F. N. also acknowledges the CNPq and INEO. SGM and LMH thank the EPSRC for funding under a Prosperity Partnership (EP/S004947/1). D.P.F. acknowledges the support of the National Science Foundation under Grant No. DMR-1848371. A.H. acknowledges the Swiss National Science Foundation, project number 200020-185041.

## References

- (1) Stranks, S. D.; Eperon, G. E.; Grancini, G.; Menelaou, C.; Alcocer, M. J. P.; Leijtens, T.; Herz, L. M.; Petrozza, A.; Snaith, H. J. Electron-Hole Diffusion Lengths Exceeding 1 Micrometer in an Organometal Trihalide Perovskite Absorber. *Science*. **2013**, 342

(6156), 341–344.

(2) Xing, G.; Mathews, N.; Sun, S.; Lim, S. S.; Lam, Y. M.; Graetzel, M.; Mhaisalkar, S.; Sum, T. C. Long-Range Balanced Electron-and Hole-Transport Lengths in Organic-Inorganic  $\text{CH}_3\text{NH}_3\text{PbI}_3$ . *Science*. **2013**, *342* (6156), 344–347.

(3) Shi, D.; Adinolfi, V.; Comin, R.; Yuan, M.; Alarousu, E.; Buin, A.; Chen, Y.; Hoogland, S.; Rothenberger, A.; Katsiev, K.; et al. Low Trap-State Density and Long Carrier Diffusion in Organolead Trihalide Perovskite Single Crystals. *Science*. **2015**, *347* (6221), 519–522.

(4) De Wolf, S.; Holovsky, J.; Moon, S. J.; Loper, P.; Niesen, B.; Ledinsky, M.; Haug, F. J.; Yum, J. H.; Ballif, C. Organometallic Halide Perovskites: Sharp Optical Absorption Edge and Its Relation to Photovoltaic Performance. *J. Phys. Chem. Lett.* **2014**, *5* (6), 1035–1039.

(5) Noh, J. H.; Im, S. H.; Heo, J. H.; Mandal, T. N.; Seok, S. Il. Chemical Management for Colorful, Efficient, and Stable Inorganic–Organic Hybrid Nanostructured Solar Cells. *Nano Lett.* **2013**, *13* (4), 1764–1769.

(6) Kojima, A.; Teshima, K.; Shirai, Y.; Miyasaka, T. Organometal Halide Perovskites as Visible-Light Sensitizers for Photovoltaic Cells. *J. Am. Chem. Soc.* **2009**, *131* (17), 6050–6051.

(7) NREL. Best Research-Cell Efficiencies. 2020.

(8) Saliba, M.; Matsui, T.; Seo, J.-Y.; Domanski, K.; Correa-Baena, J.-P.; Nazeeruddin, M. K.; Zakeeruddin, S. M.; Tress, W.; Abate, A.; Hagfeldt, A.; et al. Cesium-Containing Triple Cation Perovskite Solar Cells: Improved Stability, Reproducibility

and High Efficiency. *Energy Environ. Sci.* **2016**, *9* (6), 1989–1997.

(9) Yavari, M.; Mazloum-Ardakani, M.; Gholipour, S.; Tavakoli, M. M.; Turren-Cruz, S. H.; Taghavinia, N.; Grätzel, M.; Hagfeldt, A.; Saliba, M. Greener, Nonhalogenated Solvent Systems for Highly Efficient Perovskite Solar Cells. *Adv. Energy Mater.* **2018**, *8* (21), 1–7.

(10) Saliba, M.; Correa-Baena, J. P.; Grätzel, M.; Hagfeldt, A.; Abate, A. Perovskite Solar Cells: From the Atomic Level to Film Quality and Device Performance. *Angew. Chemie - Int. Ed.* **2018**, *57* (10), 2554–2569.

(11) Liu, C.; Sun, J.; Tan, W. L.; Lu, J.; Gengenbach, T. R.; McNeill, C. R.; Ge, Z.; Cheng, Y. B.; Bach, U. Alkali Cation Doping for Improving the Structural Stability of 2D Perovskite in 3D/2D PSCs. *Nano Lett.* **2020**, *20* (2), 1240–1251.

(12) Cao, J.; Tao, S. X.; Bobbert, P. A.; Wong, C. P.; Zhao, N. Interstitial Occupancy by Extrinsic Alkali Cations in Perovskites and Its Impact on Ion Migration. *Adv. Mater.* **2018**, *30* (26), 1–9.

(13) Saliba, M.; Matsui, T.; Domanski, K.; Seo, J.-Y.; Ummadisingu, A.; Zakeeruddin, S. M.; Correa-Baena, J.-P.; Tress, W. R.; Abate, A.; Hagfeldt, A.; et al. Incorporation of Rubidium Cations into Perovskite Solar Cells Improves Photovoltaic Performance. *Science*. **2016**, *354* (6309), 206–209.

(14) Park, I. J.; Seo, S.; Park, M. A.; Lee, S.; Kim, D. H.; Zhu, K.; Shin, H.; Kim, J. Y. Effect of Rubidium Incorporation on the Structural, Electrical, and Photovoltaic Properties of Methylammonium Lead Iodide-Based Perovskite Solar Cells. *ACS Appl. Mater. Interfaces* **2017**, *9* (48), 41898–41905.

(15) Zhang, M.; Yun, J. S.; Ma, Q.; Zheng, J.; Lau, C. F. J.; Deng, X.; Kim, J.; Kim, D.; Seidel, J.; Green, M. A.; et al. High-Efficiency Rubidium-Incorporated Perovskite Solar Cells by Gas Quenching. *ACS Energy Lett.* **2017**, *2* (2), 438–444.

(16) Turren-Cruz, S.-H.; Hagfeldt, A.; Saliba, M. Methylammonium-Free, High-Performance, and Stable Perovskite Solar Cells on a Planar Architecture. *Science*. **2018**, *362* (6413), 449–453.

(17) Patil, J. V.; Mali, S. S.; Hong, C. K. A-Site Rubidium Cation Incorporated  $\text{CsPbI}_2\text{Br}$  All-Inorganic Perovskite Solar Cells Exceeding 17% Efficiency. *Sol. RRL* **2020**, *4*, 2000164.

(18) Zhang, W.; Xiong, J.; Li, J.; Daoud, W. A. Guanidinium Passivation for Air-Stable Rubidium-Incorporated  $\text{Cs}(1-x)\text{RbxPbI}_2\text{Br}$  Inorganic Perovskite Solar Cells. *Sol. RRL* **2020**, *4*, 2000112.

(19) Hu, Y.; Hutter, E. M.; Rieder, P.; Grill, I.; Hanisch, J.; Aygüler, M. F.; Hufnagel, A. G.; Handloser, M.; Bein, T.; Hartschuh, A.; et al. Understanding the Role of Cesium and Rubidium Additives in Perovskite Solar Cells: Trap States, Charge Transport, and Recombination. *Adv. Energy Mater.* **2018**, *8* (16).

(20) Kubicki, D. J.; Prochowicz, D.; Hofstetter, A.; Zakeeruddin, S. M.; Grätzel, M.; Emsley, L. Phase Segregation in Cs-, Rb- and K-Doped Mixed-Cation  $(\text{MA})_x(\text{FA})_{1-x}\text{PbI}_3$  Hybrid Perovskites from Solid-State NMR. *J. Am. Chem. Soc.* **2017**, *139* (40), 14173–14180.

(21) Hu, Y.; Aygüler, M. F.; Petrus, M. L.; Bein, T.; Docampo, P. Impact of Rubidium and Cesium Cations on the Moisture Stability of Multiple-Cation Mixed-Halide Perovskites. *ACS Energy Lett.* **2017**, *2* (10), 2212–2218.

(22) Turren-Cruz, S.-H.; Saliba, M.; Mayer, M. T.; Juarez-Santiesteban, H.; Mathew, X.; Nienhaus, L.; Tress, W.; Erodici, M. P.; Sher, M.-J.; Bawendi, M. G.; et al. Enhanced Charge Carrier Mobility and Lifetime Suppress Hysteresis and Improve Efficiency in Planar Perovskite Solar Cells. *Energy Environ. Sci.* **2018**, *11* (1), 78–86.

(23) Cao, J.; Tao, S. X.; Bobbert, P. A.; Wong, C.-P.; Zhao, N. Interstitial Occupancy by Extrinsic Alkali Cations in Perovskites and Its Impact on Ion Migration. *Adv. Mater.* **2018**, *30* (26), 1707350.

(24) Tang, Z.; Uchida, S.; Bessho, T.; Kinoshita, T.; Wang, H.; Awai, F.; Jono, R.; Maitani, M. M.; Nakazaki, J.; Kubo, T.; et al. Modulations of Various Alkali Metal Cations on Organometal Halide Perovskites and Their Influence on Photovoltaic Performance. *Nano Energy* **2018**, *45*, 184–192.

(25) Qiao, L.; Fang, W.-H.; Long, R.; Prezhdo, O. V. Extending Carrier Lifetimes in Lead Halide Perovskites with Alkali Metals by Passivating and Eliminating Halide Interstitial Defects. *Angew. Chemie Int. Ed.* **2020**, *59* (12), 4684–4690.

(26) Dang, H. X.; Wang, K.; Ghasemi, M.; Tang, M.-C.; De Bastiani, M.; Aydin, E.; Dauzon, E.; Barrit, D.; Peng, J.; Smilgies, D.-M.; et al. Multi-Cation Synergy Suppresses Phase Segregation in Mixed-Halide Perovskites. *Joule* **2019**, *3* (7), 1746–1764.

(27) Qin, M.; Tse, K.; Lau, T.; Li, Y.; Su, C.; Yang, G.; Chen, J.; Zhu, J.; Jeng, U.; Li, G.; et al. Manipulating the Mixed-Perovskite Crystallization Pathway Unveiled by In Situ GIWAXS. *Adv. Mater.* **2019**, *1901284*.

(28) Yan, K.; Long, M.; Zhang, T.; Wei, Z.; Chen, H.; Yang, S.; Xu, J. Hybrid Halide Perovskite Solar Cell Precursors: Colloidal Chemistry and Coordination Engineering

behind Device Processing for High Efficiency. *J. Am. Chem. Soc.* **2015**, *137* (13), 4460–4468.

(29) McMeekin, D. P.; Wang, Z.; Rehman, W.; Pulvirenti, F.; Patel, J. B.; Noel, N. K.; Johnston, M. B.; Marder, S. R.; Herz, L. M.; Snaith, H. J. Crystallization Kinetics and Morphology Control of Formamidinium–Cesium Mixed-Cation Lead Mixed-Halide Perovskite via Tunability of the Colloidal Precursor Solution. *Adv. Mater.* **2017**, *29* (29), 1607039.

(30) Sharenko, A.; Mackeen, C.; Jewell, L.; Bridges, F.; Toney, M. F. Evolution of Iodoplumbate Complexes in Methylammonium Lead Iodide Perovskite Precursor Solutions. *Chem. Mater.* **2017**, *29* (3), 1315–1320.

(31) Abdi-Jalebi, M.; Andaji-Garmaroudi, Z.; Cacovich, S.; Stavrakas, C.; Philippe, B.; Richter, J. M.; Alsari, M.; Booker, E. P.; Hutter, E. M.; Pearson, A. J.; et al. Maximizing and Stabilizing Luminescence from Halide Perovskites with Potassium Passivation. *Nature* **2018**, *555* (7697), 497–501.

(32) Yang, W. S.; Park, B.-W.; Jung, E. H.; Jeon, N. J.; Kim, Y. C.; Lee, D. U.; Shin, S. S.; Seo, J.; Kim, E. K.; Noh, J. H.; et al. Iodide Management in Formamidinium-Lead-Halide-Based Perovskite Layers for Efficient Solar Cells. *Science (80- ).* **2017**, *356* (6345), 1376–1379.

(33) Correa-Baena, J.-P.; Luo, Y.; Brenner, T. M.; Snaider, J.; Sun, S.; Li, X.; Jensen, M. A.; Hartono, N. T. P.; Nienhaus, L.; Wieghold, S.; et al. Homogenized Halides and Alkali Cation Segregation in Alloyed Organic-Inorganic Perovskites. *Science (80- ).* **2019**, *363* (6427), 627–631.

(34) Alharbi, E. A.; Alyamani, A. Y.; Kubicki, D. J.; Uhl, A. R.; Walder, B. J.; Alanazi, A.

Q.; Luo, J.; Burgos-Caminal, A.; Albadri, A.; Albritthen, H.; et al. Atomic-Level Passivation Mechanism of Ammonium Salts Enabling Highly Efficient Perovskite Solar Cells. *Nat. Commun.* **2019**, *10* (1), 3008.

(35) Jiang, Q.; Zhao, Y.; Zhang, X.; Yang, X.; Chen, Y.; Chu, Z.; Ye, Q.; Li, X.; Yin, Z.; You, J. Surface Passivation of Perovskite Film for Efficient Solar Cells. *Nat. Photonics* **2019**, *13* (7), 460–466.

(36) Bouduban, M. E. F.; Queloz, V. I. E.; Caselli, V. M.; Cho, K. T.; Kirmani, A. R.; Paek, S.; Roldan-Carmona, C.; Richter, L. J.; Moser, J. E.; Savenije, T. J.; et al. Crystal Orientation Drives the Interface Physics at Two/Three-Dimensional Hybrid Perovskites. *J. Phys. Chem. Lett.* **2019**, *10* (19), 5713–5720.

(37) Beal, R. E.; Hagström, N. Z.; Barrier, J.; Gold-Parker, A.; Prasanna, R.; Bush, K. A.; Passarello, D.; Schelhas, L. T.; Brüning, K.; Tassone, C. J.; et al. Structural Origins of Light-Induced Phase Segregation in Organic-Inorganic Halide Perovskite Photovoltaic Materials. *Matter* **2020**, *2* (1), 207–219.

(38) Roldán-Carmona, C.; Gratia, P.; Zimmermann, I.; Grancini, G.; Gao, P.; Graetzel, M.; Nazeeruddin, M. K. High Efficiency Methylammonium Lead Triiodide Perovskite Solar Cells: The Relevance of Non-Stoichiometric Precursors. *Energy Environ. Sci.* **2015**, *8* (12), 3550–3556.

(39) Jacobsson, T. J.; Correa-Baena, J.-P.; Halvani Anaraki, E.; Philippe, B.; Stranks, S. D.; Bouduban, M. E. F.; Tress, W.; Schenk, K.; Teuscher, J.; Moser, J.-E.; et al. Unreacted PbI<sub>2</sub> as a Double-Edged Sword for Enhancing the Performance of Perovskite Solar Cells. *J. Am. Chem. Soc.* **2016**, *138* (32), 10331–10343.

(40) Bi, D.; Tress, W.; Dar, M. I.; Gao, P.; Luo, J.; Renevier, C.; Schenk, K.; Abate, A.;

Giordano, F.; Correa Baena, J.-P.; et al. Efficient Luminescent Solar Cells Based on Tailored Mixed-Cation Perovskites. *Sci. Adv.* **2016**, *2* (1), e1501170-e1501170.

(41) Yoo, J. J.; Wieghold, S.; Sponseller, M. C.; Chua, M. R.; Bertram, S. N.; Hartono, N. T. P.; Tresback, J. S.; Hansen, E. C.; Correa-Baena, J.-P.; Bulović, V.; et al. An Interface Stabilized Perovskite Solar Cell with High Stabilized Efficiency and Low Voltage Loss. *Energy Environ. Sci.* **2019**, *12* (7), 2192–2199.

(42) Johnston, M. B.; Herz, L. M. Hybrid Perovskites for Photovoltaics: Charge-Carrier Recombination, Diffusion, and Radiative Efficiencies. *Acc. Chem. Res.* **2016**, *49* (1), 146–154.

(43) Greenland, C.; Shnier, A.; Rajendran, S. K.; Smith, J. A.; Game, O. S.; Wamwangi, D.; Turnbull, G. A.; Samuel, I. D. W.; Billing, D. G.; Lidzey, D. G. Correlating Phase Behavior with Photophysical Properties in Mixed-Cation Mixed-Halide Perovskite Thin Films. *Adv. Energy Mater.* **2020**, *10* (4), 1901350.

(44) Wehrenfennig, C.; Eperon, G. E.; Johnston, M. B.; Snaith, H. J.; Herz, L. M. High Charge Carrier Mobilities and Lifetimes in Organolead Trihalide Perovskites. *Adv. Mater.* **2014**, *26* (10), 1584–1589.

(45) Motti, S. G.; Crothers, T.; Yang, R.; Cao, Y.; Li, R.; Johnston, M. B.; Wang, J.; Herz, L. M. Heterogeneous Photon Recycling and Charge Diffusion Enhance Charge Transport in Quasi-2D Lead-Halide Perovskite Films. *Nano Lett.* **2019**, *19* (6), 3953–3960.

(46) Park, S. M.; Abtahi, A.; Boehm, A. M.; Graham, K. R. Surface Ligands for Methylammonium Lead Iodide Films: Surface Coverage, Energetics, and Photovoltaic Performance. *ACS Energy Lett.* **2020**, *5* (3), 799–806.

(47) Doherty, T. A. S.; Winchester, A. J.; Macpherson, S.; Johnstone, D. N.; Pareek, V.; Tennyson, E. M.; Kosar, S.; Kosasih, F. U.; Anaya, M.; Abdi-Jalebi, M.; et al. Performance-Limiting Nanoscale Trap Clusters at Grain Junctions in Halide Perovskites. *Nature* **2020**, *580* (7803), 360–366.

(48) Saidaminov, M. I.; Williams, K.; Wei, M.; Johnston, A.; Quintero-Bermudez, R.; Vafaie, M.; Pina, J. M.; Proppe, A. H.; Hou, Y.; Walters, G.; et al. Multi-Cation Perovskites Prevent Carrier Reflection from Grain Surfaces. *Nat. Mater.* **2020**, *19* (4), 412–418.

(49) Ambrosio, F.; Meggiolaro, D.; Mosconi, E.; De Angelis, F. Charge Localization and Trapping at Surfaces in Lead-Iodide Perovskites: The Role of Polarons and Defects. *J. Mater. Chem. A* **2020**, *8* (14), 6882–6892.

(50) Motti, S. G.; Meggiolaro, D.; Barker, A. J.; Mosconi, E.; Perini, C. A. R.; Ball, J. M.; Gandini, M.; Kim, M.; De Angelis, F.; Petrozza, A. Controlling Competing Photochemical Reactions Stabilizes Perovskite Solar Cells. *Nat. Photonics* **2019**, *13* (8), 532–539.

(51) Whalley, L. D.; Crespo-Otero, R.; Walsh, A. H-Center and V-Center Defects in Hybrid Halide Perovskites. *ACS Energy Lett.* **2017**, *2* (12), 2713–2714.

(52) Li, W.; Liu, J.; Bai, F.-Q.; Zhang, H.-X.; Prezhdo, O. V. Hole Trapping by Iodine Interstitial Defects Decreases Free Carrier Losses in Perovskite Solar Cells: A Time-Domain Ab Initio Study. *ACS Energy Lett.* **2017**, *2* (6), 1270–1278.

(53) Meggiolaro, D.; Mosconi, E.; De Angelis, F. Mechanism of Reversible Trap Passivation by Molecular Oxygen in Lead-Halide Perovskites. *ACS Energy Lett.* **2017**, *2* (12), 2794–2798.

(54) Xu, J.; Buin, A.; Ip, A. H.; Li, W.; Voznyy, O.; Comin, R.; Yuan, M.; Jeon, S.; Ning, Z.; McDowell, J. J.; et al. Perovskite–Fullerene Hybrid Materials Suppress Hysteresis in Planar Diodes. *Nat. Commun.* **2015**, *6* (1), 7081.

(55) He, J.; Fang, W.-H.; Long, R. Unravelling the Effects of Oxidation State of Interstitial Iodine and Oxygen Passivation on Charge Trapping and Recombination in CH<sub>3</sub>NH<sub>3</sub>PbI<sub>3</sub> Perovskite: A Time-Domain Ab Initio Study. *Chem. Sci.* **2019**, *10* (43), 10079–10088.

(56) Hartono, N. T. P.; Sun, S.; Gélvez-Rueda, M. C.; Pierone, P. J.; Erodici, M. P.; Yoo, J.; Wei, F.; Bawendi, M.; Grozema, F. C.; Sher, M.; et al. The Effect of Structural Dimensionality on Carrier Mobility in Lead-Halide Perovskites. *J. Mater. Chem. A* **2019**, *7* (41), 23949–23957.

(57) Li, X.; Chen, C.-C.; Cai, M.; Hua, X.; Xie, F.; Liu, X.; Hua, J.; Long, Y.-T.; Tian, H.; Han, L. Efficient Passivation of Hybrid Perovskite Solar Cells Using Organic Dyes with  $\square$ COOH Functional Group. *Adv. Energy Mater.* **2018**, *8* (20), 1800715.

(58) Guan, L.; Jiao, N.; Guo, Y. Trap-State Passivation by Nonvolatile Small Molecules with Carboxylic Acid Groups for Efficient Planar Perovskite Solar Cells. *J. Phys. Chem. C* **2019**, *123* (23), 14223–14228.

(59) Luo, B.; Naghadeh, S. B.; Allen, A.; Li, X.; Zhang, J. Z. Peptide-Passivated Lead Halide Perovskite Nanocrystals Based on Synergistic Effect between Amino and Carboxylic Functional Groups. *Adv. Funct. Mater.* **2017**, *27* (6), 1604018.

(60) Yang, S.; Dai, J.; Yu, Z.; Shao, Y.; Zhou, Y.; Xiao, X.; Zeng, X. C.; Huang, J. Tailoring Passivation Molecular Structures for Extremely Small Open-Circuit Voltage Loss in Perovskite Solar Cells. *J. Am. Chem. Soc.* **2019**, *141* (14), 5781–5787.

(61) Liu, L.; Huang, S.; Lu, Y.; Liu, P.; Zhao, Y.; Shi, C.; Zhang, S.; Wu, J.; Zhong, H.; Sui, M.; et al. Grain-Boundary “Patches” by In Situ Conversion to Enhance Perovskite Solar Cells Stability. *Adv. Mater.* **2018**, *30* (29), 1800544.

(62) Kim, S.; Bae, S.; Lee, S.-W.; Cho, K.; Lee, K. D.; Kim, H.; Park, S.; Kwon, G.; Ahn, S.-W.; Lee, H.-M.; et al. Relationship between Ion Migration and Interfacial Degradation of  $\text{CH}_3\text{NH}_3\text{PbI}_3$  Perovskite Solar Cells under Thermal Conditions. *Sci. Rep.* **2017**, *7* (1), 1200.